

Resonant inelastic x-ray scattering investigation of the crystal-field splitting of Sm^{3+} in SmB_6

Andrea Amorese,^{1,2} Oliver Stockert,² Kurt Kummer,³ Nicholas B. Brookes,³ Dae-Jeong Kim,⁴ Zachary Fisk,⁴ Maurits W. Haverkort,⁵ Peter Thalmeier,² Liu Hao Tjeng,² and Andrea Severing^{1,2}

¹*Institute of Physics II, University of Cologne, Zùlpicher Straße 77, 50937 Cologne, Germany*

²*Max Planck Institute for Chemical Physics of Solids, Nöthnitzer Straße 40, 01187 Dresden, Germany*

³*European Synchrotron Radiation Facility, 71 Avenue des Martyrs, CS40220, F-38043 Grenoble Cedex 9, France*

⁴*Department of Physics and Astronomy, University of California, Irvine, California 92697, USA*

⁵*Institute for Theoretical Physics, Heidelberg University, Philosophenweg 19, 69120 Heidelberg, Germany*

 (Received 29 January 2019; revised manuscript received 25 November 2019; published 13 December 2019)

The crystal-field (CF) splitting of the ${}^6H_{5/2}$ Hund's rule ground state of Sm^{3+} in the strongly correlated topological insulator SmB_6 has been determined with high-resolution resonant inelastic x-ray scattering (RIXS) at the $\text{Sm } M_5$ edge. The valence selectivity of RIXS allows isolating the crystal-field-split excited multiplets of the Sm^{3+} ($4f^5$) configuration from those of Sm^{2+} ($4f^6$) in intermediate valent SmB_6 . We find that the quartet Γ_8 ground state and the doublet Γ_7 excited state are split by $\Delta_{6H_{5/2}}^{\text{CF}} = 20 \pm 10$ meV which sets an upper limit for the $4f$ bandwidth. This indicates an extremely large mass renormalization from the band-structure value, pointing out the need to consider the coefficients of fractional parentage for the hopping of the $4f$ electrons. The tiny bandwidth explains the small value of the indirect gap and puts constraints on the energies of the topological surface states.

DOI: [10.1103/PhysRevB.100.241107](https://doi.org/10.1103/PhysRevB.100.241107)

I. INTRODUCTION

SmB_6 is an intermediate valent Kondo insulator in which the hybridization of localized $4f$ electrons and the conduction band (cf hybridization) leads to the formation of a gap Δ_h [1–5] of the order of 20 meV [6–11]. Accordingly, the resistivity increases with decreasing temperature but instead of diverging it reaches a plateau below about 10 K. Surface states could be an explanation for the finite low temperature conductivity [12–19] and indeed it was theoretically predicted that SmB_6 has all the ingredients, such as strong spin-orbit coupling and electrons of opposite parity (d and f), for being a strongly correlated topological insulator [20–24]. This prediction initiated many studies such as angle-resolved photoelectron spectroscopy (ARPES) [6–11,25–29], scanning tunneling spectroscopy [30–33], or de Haas–van Alphen [34–36]. Yet, despite all these efforts, the exciting question whether these surface states are topologically nontrivial still remains to be answered, which may be caused by the complications of the SmB_6 surface [7,31,32].

Band-structure calculations have been very successful in the field of semiconducting topological insulators, but they are not adequate for the rare earths because of correlations, nor are they accurate enough because the energy scales are much smaller. For example, several density functional theory calculations imply that the hole of the Sm^{3+} $4f^5$ configuration resides in the doublet Γ_7 [22,37–40] but a recent hard x-ray *nonresonant* inelastic x-ray scattering (NIXS) investigation [41,42] by some of the authors of the present study reveals that the ground-state symmetry is the Γ_8 quartet. Along the same line, band-structure calculations produce $4f$ bandwidths of several hundred meV, while so far no $4f$ bulk dispersions in ARPES have been observed within the experimental

resolution [6–11,25–29]. The inclusion of correlation effects using Gutzwiller or dynamical mean-field approaches (DMFT) [22,43] does produce narrower bands (about 80 and 20 meV, respectively), but it is not clear whether the mass renormalizations used or found are realistic, with consequences for the prediction of the energies of the topological surface states [16,21–23].

To better understand the many-body aspects of SmB_6 and to help the search for the topological surface states, we follow here a different strategy. We will determine the energy scales of the low-lying bulk states which will also provide information about the surface since its topology is given by the bulk. We will look in particular at the $4f$ crystal field (CF). Knowing that the ground state is given by a pure Γ_8 state [41,42], we can use the value of the CF splitting as an upper limit of the $4f$ bandwidth, of the band gap, and also of the energies of the topological surface states as we will explain below.

SmB_6 has a valence of about 2.5–2.7 at low temperatures [44–48], so that the electronic state of Sm is described by the Hund's rule ground states of the Sm $4f^6$ ($2+$) and Sm $4f^5$ ($3+$) configurations. The two low-lying multiplets of the $4f^6$ with the total angular momenta $J = 0$ and $J = 1$ are not CF split and their wave functions are spherical [49]. The lowest energy multiplet ${}^6H_{5/2}$ of the $4f^5$ configuration, however, is split into a Γ_8 quartet and Γ_7 doublet whereby the splitting energy, $\Delta_{6H_{5/2}}^{\text{CF}}$, eluded its determination until today. Band-structure calculations predicted energy scales of about 100 meV (see, e.g. [39,40]) although an extrapolation of the CF parameters within the RB_6 ($R = \text{rare earth}$) series suggests a $\Delta_{6H_{5/2}}^{\text{CF}}$ of the order of 15 meV; an extrapolation that is, of course, only valid in diluted systems [50,51].

Inelastic neutron scattering (INS) is the obvious technique for measuring $\Delta_{6H_{5/2}}^{\text{CF}}$, but here INS has not been successful because of the strong neutron absorption of Sm and B even in double isotopic samples, the superposition of both Sm configurations, and the presence of *cf* hybridization. INS yields nevertheless the following important information: the observation of the *spin-orbit* transitions ${}^7F_0 \rightarrow {}^7F_1$ and ${}^6H_{5/2} \rightarrow {}^6H_{7/2}$ at ≈ 35 meV and ≈ 130 meV, the existence of a long-living spin resonance at about 14 meV at the *X* and *R* high-symmetry points with a non-*4f*-like form factor that decays above 30 K, and the occurrence of quasielastic magnetic scattering ($\Gamma/2 \approx 10$ meV HWHM) at 100 K that follows the Sm^{3+} form factor [53–57].

Here resonant inelastic x-ray scattering (RIXS) is a promising option [58,59]. RIXS is bulk sensitive, much more so than ARPES and scanning tunneling microscopy/scanning tunneling spectroscopy, it is element specific, and above all, it is also configuration selective. This is well known from studying valences at the rare-earth *L* edge in the so-called partial fluorescence yield mode [60,61]. We use the configuration selectivity at the $M_{4,5}$ edge ($3d \rightarrow 4f$) to distinguish the excitation spectra of the two Sm configurations.

II. METHOD

Figure 1 shows the M_5 -edge RIXS process for SmB_6 . The initial state configuration is an admixture of Sm^{2+} : $3d^{10}4f^6$

(red) and Sm^{3+} : $3d^{10}4f^5$ (blue). The resonant absorption of an ≈ 1090 eV x-ray photon at the M_5 edge ($3d_{5/2} \rightarrow 4f$) creates a core hole. In this intermediate state the absorption lines of the two configurations are split in energy due to the different impact of the core hole potential on either configuration. Finally, in RIXS spectroscopy the intensity of the photons emitted by the resonant radiative decay is monitored as a function of the outgoing photon energy ($\hbar\omega_{\text{out}}$) so that energy transfer spectra can be measured. In principle the decay process in the RIXS process of SmB_6 yields the superposition of two multiplet spectra [see simulations of two independent configurations in Fig. 1(b)] but the choice of the incident photon energy $\hbar\omega_{\text{in}}$ along the x-ray absorption spectrum (XAS) edge allows enhancing the signal of one of the two configurations. It is possible to resolve the CF splittings in a RIXS experiment because the large lifetime broadening of the intermediate state does not enter, i.e., the lifetime broadening in RIXS that matters is that of the final state [62–65].

Figure 1(b) shows calculations of the RIXS spectra for pure Sm^{2+} (red) and pure Sm^{3+} (blue). The photon-in photon-out RIXS process yields the selection rule $\Delta J = 0, \pm 1, \pm 2$ so that multiplets with $J = 0, 1, 2$ (for Sm^{2+}) and $J = 1/2, 3/2, 5/2, 7/2,$ and $9/2$ (for Sm^{3+}) are accessible, the latter ones being so weak that they are not shown. In the cubic point symmetry of SmB_6 only multiplets with $J \geq 2$ are CF split as shown on an enlarged energy scale in the colored boxes of Fig. 1(b).

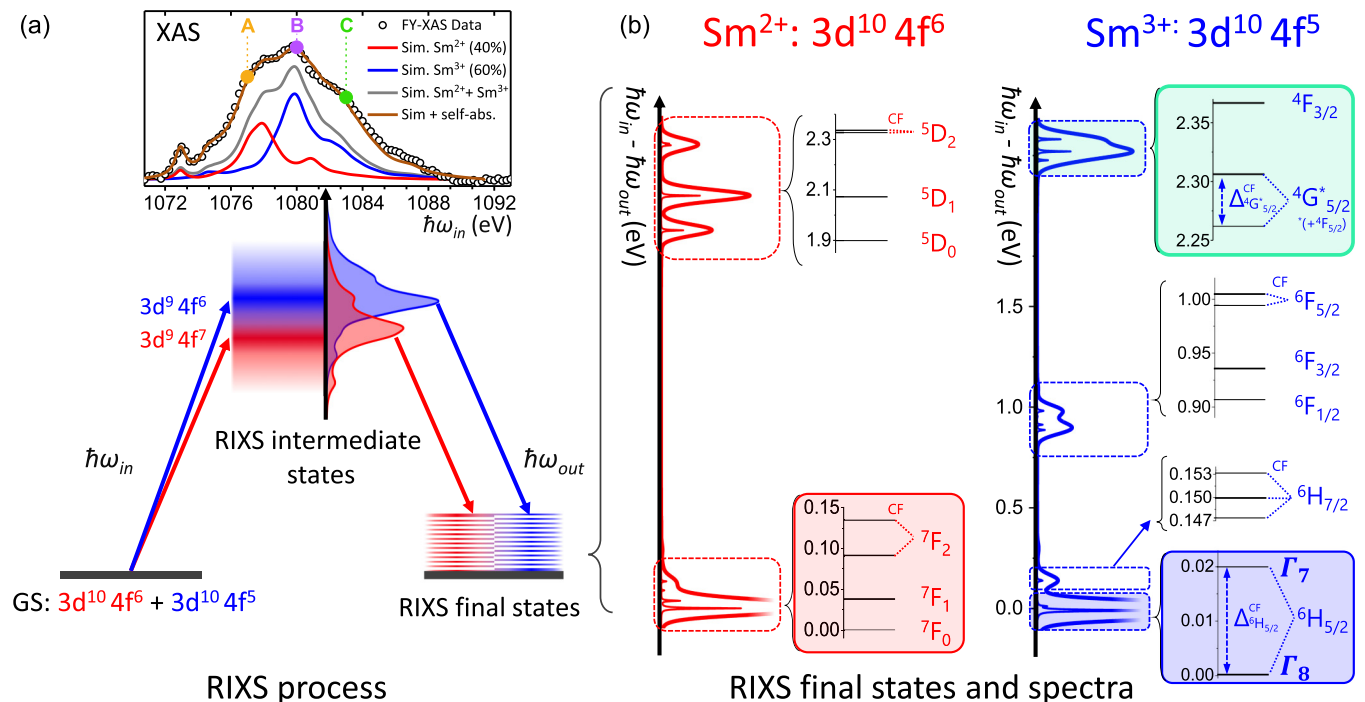


FIG. 1. (a) RIXS process at the $\text{Sm } M_5$ edge ($3d \rightarrow 4f$) from mixed ground state, $4f^6$ (red) and $4f^5$ (blue) (see text). Inset: Experimental, bulk sensitive fluorescence-yield x-ray absorption spectrum (FY-XAS) of the $\text{Sm } M_5$ edge of SmB_6 (black circles), the XAS simulation (gray line) decomposed into 60% Sm^{3+} (blue line) and 40% Sm^{2+} (red line) spectral weights according to valence measurements [44–48], plus simulation including self-absorption (brown line) [52]; all scaled down by a factor of 3 for graphical clarity. The colored dots **A**, **B**, and **C** show the incident energies $\hbar\omega_{\text{in}}$ of the RIXS experiment. (b) Calculated RIXS spectra ($\hbar\omega_{\text{in}} - \hbar\omega_{\text{out}}$) of Sm^{2+} (red, $\hbar\omega_{\text{in}} = \text{B}$) and Sm^{3+} (blue, $\hbar\omega_{\text{in}} = \text{C}$) for the geometry as in Fig. 4(a) and vertical (σ) incoming polarization. Multiplet as well as expected crystal-field splittings are shown on an expanded scale in the red, blue, and green boxes. Thicker lines stand for higher degeneracies. The splitting $\Delta_{4G_{5/2}}^{\text{CF}}$ (green box) is used for determining $\Delta_{6H_{5/2}}^{\text{CF}}$ (blue box).

Apart from the valence selectivity, another advantage of RIXS is that the transferred energy is, in contrast to INS, practically unlimited, i.e., with RIXS we can study higher-lying multiplets instead of the strongly hybridized Hund's rule ground state of Sm^{3+} [blue box in Fig. 1(b)]. We will show that we can take advantage of the CF effect on the ${}^4G_{5/2}^*$ multiplet at about 2.4 eV [see the green box in Fig. 1(b)]. The asterisk indicates that due to the particularly strong intermultiplet mixing acting on this level, L is no longer a good quantum number so that the multiplet labeling is not strictly valid. The total angular momentum $J = 5/2$, however, remains a good quantum number for CF splittings smaller than the spin-orbit splittings. ${}^4G_{5/2}^*$ and the Hund's rule ground state ${}^6H_{5/2}$ have the same J so that the same CF parameter \tilde{A}_4^0 [66] (together with $\tilde{A}_4^4 = \sqrt{5/14}\tilde{A}_4^0$) determines the CF splitting. The size of the splitting is given by $\tilde{A}_4^0 \cdot \tilde{\beta}_{\text{JLS}}$ whereby $\tilde{\beta}_{\text{JLS}}$ is something like a Stevens factor that is calculated within the full multiplet routine, while \tilde{A}_4^0 is determined experimentally. Hence, we can gain information on the splitting of the lowest-energy ${}^6H_{5/2}$ multiplet by fitting the RIXS signal of the ${}^4G_{5/2}^*$ multiplet. For ${}^4G_{5/2}^*$ the $\tilde{\beta}_{\text{JLS}}$ factor is larger than for ${}^6H_{5/2}$ (approximately double) so that the CF splitting is larger and less hampered by the limited energy resolution at the $\text{Sm } M_5$ edge. In addition, the signal is free of the strong tail of the elastic peak (at 0 eV) and of the signal from other low-energy excitations.

III. EXPERIMENT AND SIMULATION

The RIXS experiment was performed on aluminum-flux-grown single crystals [16] that were aligned by Laue prior to the experiment.

The SmB_6 [16] M -edge RIXS experiment at 20 K was performed at the ERIXS spectrometer of the ID32 beamline [67] at the European Synchrotron Radiation Facility, Grenoble, France with a resolution of 45 meV at the $\text{Sm } M_5$ edge (≈ 1090 meV). Data were taken with two different scattering angles, namely, $2\Theta = 90^\circ$ and 150° . The samples were cleaved *in situ* under vacuum, then transferred to the main chamber and measured at 20 K. Data were acquired for about 5 h for each spectrum (only 3 h for the spectrum **B**). The instrument 45 meV-FWHM Gaussian response function was estimated by measuring a carbon tape. The measurements were performed with horizontal polarization (π) of the incident photons; two different scattering angles, $2\Theta = 90^\circ$ and $2\Theta = 150^\circ$; a sample angle of $\theta = 37.3^\circ$; and with the **b** and **c** directions of the sample in the scattering plane (see inset of Fig. 4).

Simulations were performed with the full multiplet code QUANTY [68,69]. Atomic parameters were taken from the COWAN code [70]. Figure 2 shows that the energy positions of the multiplets are very sensitive to changes of the reduction factor r_{4f-4f} of the Slater integrals so that r_{4f-4f} was determined by adjusting the energy positions of the multiplet excitations. The reduction factor r_{3d-4f} , on the other hand, affects only slightly the relative intensities of the RIXS peaks. We find that $r_{4f-4f} = r_{3d-4f} = 0.86$ provides a very good fit of the relative RIXS intensities and line positions, and to the XAS data. These values are in agreement with those in Ref. [41].

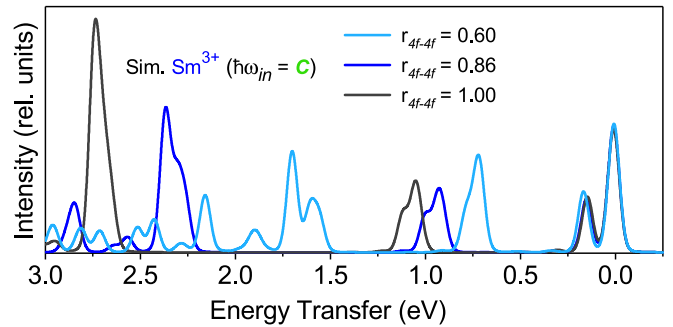


FIG. 2. RIXS simulations of Sm^{3+} for incident energy C with various reduction factors r_{4f-4f} ($r_{3d-4f} = 0.86$).

IV. RESULTS

The inset of Fig. 1(a) shows the bulk-sensitive experimental fluorescence-yield XAS (FY-XAS) data of the $\text{Sm } M_5$ edge of SmB_6 at 20 K, with the photon polarization parallel to the 100 direction (black line). These data have been simulated by calculating an XAS spectrum (gray line) containing Sm^{3+} (40%) and Sm^{2+} (60%) spectral weights according to the SmB_6 valence at low T [44–48]. Then self-absorption effects were included in the simulation (see brown line) [52] and compared with the FY-XAS data. Note, for reasons of graphical clarity the XAS data have been rescaled by a factor of 3. The orange, purple, and green dots marked **A**, **B**, and **C** indicate the incident energies that were used for the RIXS experiment.

Figure 3(a) shows the RIXS data at $T = 20$ K up to 3 eV taken with the three different incident energies $\hbar\omega_{\text{in}} = \mathbf{A}$, **B**, and **C** and a scattering angle of $2\Theta = 90^\circ$. $\hbar\omega_{\text{in}} = \mathbf{A}$ corresponds to the preedge region where the $3d \rightarrow 4f$ absorption process is dominated by the ground state of $\text{Sm}^{2+} 4f^6$. The asymmetric intensity close to the elastic line is indicative for the low-energy transitions ${}^7F_0 \rightarrow {}^7F_1$ at 35 meV and some ${}^7F_0 \rightarrow {}^7F_2$ at about 150 meV, whereas higher-energy transfers have no cross section because they require larger incident energies due to selection rules. At $\hbar\omega_{\text{in}} = \mathbf{C}$ the absorption arises mainly from the $4f^5$ ground state of Sm^{3+} . Energy **B** is in-between, i.e., the RIXS spectrum shows features characteristic of both valences but is not simply the superposition of spectra **A** and **C** because of the incident energy dependence of the accessible excitations. Figure 3(b) shows full multiplet RIXS calculations for the same spectrometer configuration for Sm^{2+} with the incident energies **B** (dotted red line) and **C** (red solid line) and for Sm^{3+} with incident energy **C** (solid blue line). The comparison of both panels demonstrates the energy selectivity of the RIXS signal and it confirms that the spectrum measured with $\hbar\omega_{\text{in}} = \mathbf{C}$ resembles almost purely Sm^{3+} multiplets. We will therefore focus on the region of the ${}^4F_{3/2}$ and ${}^4G_{5/2}^*$ multiplets measured with this incident energy for further analysis of the crystal-field problem of Sm^{3+} [see colored regions in Fig. 3(b)].

The top of Figs. 4(a) and 4(b) shows the RIXS data of the ${}^4F_{3/2}$ and ${}^4G_{5/2}^*$ multiplets (dark-blue dots) at around 2.4 eV energy transfer ($\hbar\omega_{\text{in}} = \mathbf{C}$) measured with horizontal (π) polarization and two different scattering angles, $2\theta = 90^\circ$ and 150° , thus taking advantage of the cross-section dependence on the scattering geometry. We recall that the multiplet ${}^4F_{3/2}$

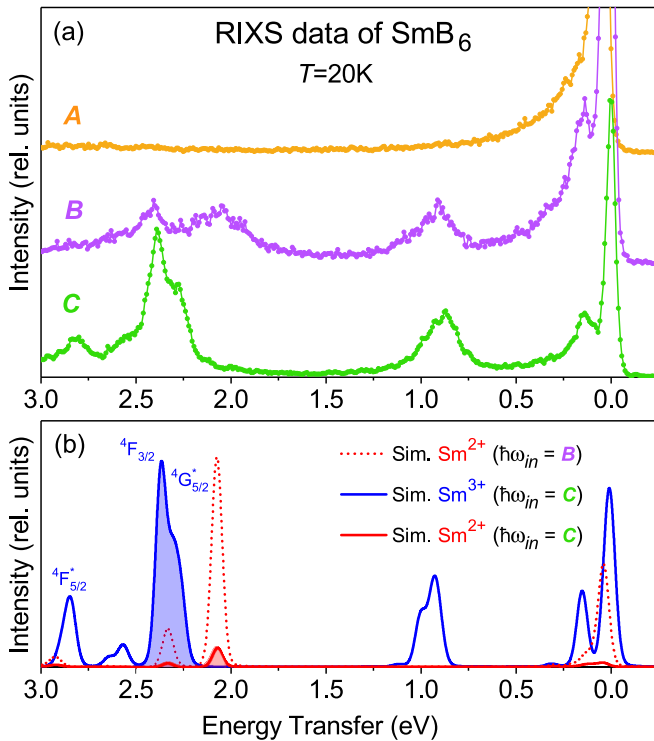


FIG. 3. (a) RIXS data of SmB_6 for incident energies $\hbar\omega_{\text{in}}$ **A**, **B**, and **C** as defined in Fig. 1(a) (see text for the scattering geometry). (b) RIXS simulation for Sm^{3+} (solid blue line) with $\hbar\omega_{\text{in}} = \text{C}$ and for Sm^{2+} with $\hbar\omega_{\text{in}} = \text{B}$ (dashed red line) and **C** (solid red line) (simulation, see text).

is not affected by the CF because of $J < 2$ but that a finite CF splits the ${}^4G_{5/2}^*$ multiplet into two levels.

Figure 4 also shows simulations broadened with a 45 meV Gaussian resolution function for different CF splittings. We find that, for the same CF parameter, $\Delta_{4G_{5/2}^*}^{\text{CF}}$ is about 2.2 times larger than $\Delta_{6H_{5/2}}^{\text{CF}}$. We show the simulations for $\Delta_{6H_{5/2}}^{\text{CF}} = [-40, +40]$ meV in steps of 10 meV, whereby the positive numbers refer to a Γ_8 and the negative ones to a Γ_7 ground state. Here the narrow thin lines correspond to the same CF simulation but with an unrealistic small resolution in order to visualize the details of the CF splittings. The simulation with $\Delta_{6H_{5/2}}^{\text{CF}} = 0$ (green lines) shows two main peaks, the ${}^4G_{5/2}^*$ multiplet and the ${}^4F_{3/2}$ about 80 meV higher in energy. We learn from these simulations that for CF splittings of less than 40 meV the intermixing of the two multiplets is negligible. We now compare data and simulations in detail: For 0 meV CF (green lines), and for +10 and -10 meV splitting (light-blue and yellow lines) and $2\Theta = 150^\circ$ the ${}^4G_{5/2}^*$ intensity would be stronger than the ${}^4F_{3/2}$ peak [see Fig. 4(b)]. This is not the case in the experiment. Hence, the CF splitting of the ground state must be larger than 10 meV. For a negative CF splitting only one ${}^4G_{5/2}^*$ CF excitation would have intensity in the $2\Theta = 90^\circ$ configuration, thus leading to a deep valley between the two multiplets which has not been observed [see Fig. 4(a)]. We therefore conclude that the splitting must be positive, i.e., we confirm the results of previous directional-dependent NIXS data [41]. For +40 meV CF splitting the spectral shape has changed considerably for both scattering geometries so

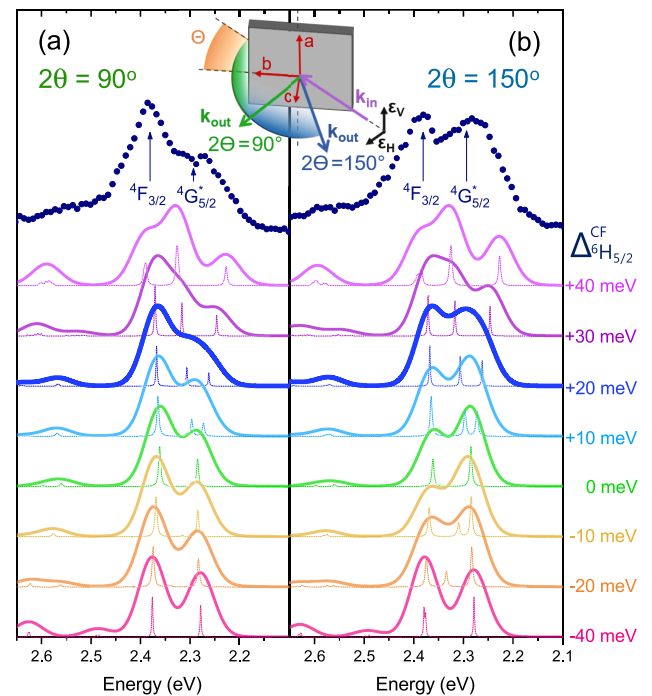


FIG. 4. Data and simulations of RIXS spectra with $\hbar\omega_{\text{in}} = \text{C}$ (dark-blue dots) with horizontal polarization (π) for two scattering angles $2\Theta = 90^\circ$ (a) and $2\Theta = 150^\circ$ (b) (see inset). Different colors are simulations with different crystal-field splittings; thin dotted lines with an unrealistic narrow resolution and solid thick lines taking into account the resolution function. The numbers refer to the respective Hund's rule ground-state splitting $\Delta_{6H_{5/2}}^{\text{CF}}$, positive numbers refer to a Γ_8 , and negative numbers to a Γ_7 ground state. Note, $\Delta_{4G_{5/2}^*}^{\text{CF}} \approx 2.2\Delta_{6H_{5/2}}^{\text{CF}}$.

we also exclude this possibility as well. It turns out that peak shapes and intensity ratios of both scattering configurations are best reproduced with $\Delta_{6H_{5/2}}^{\text{CF}} = +20$ meV.

Figure 5 shows the same RIXS data as in Fig. 4 but after subtracting a linear background. The lines represent an empirical fit with three Voigt profiles whereby the Gaussian contribution is kept fixed to the experimental resolution. The Lorentzian widths, the line positions, and intensities were varied with the simplification that the lifetime broadening and intensity of the two CF excitations are identical. The

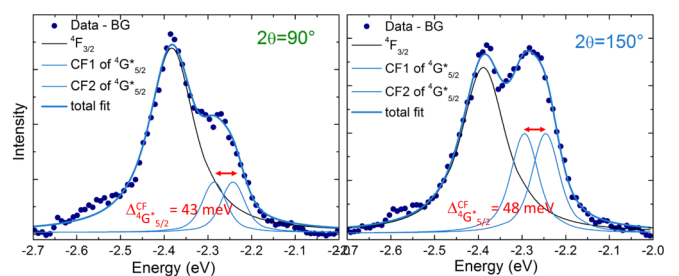


FIG. 5. Background corrected RIXS spectra of Fig. 4 with an empirical fit of three Voigt profiles (see text), one resembling the ${}^4F_{3/2}$ multiplet and two the crystal-field split ${}^4G_{5/2}^*$. The crystal-field splitting of the ${}^4G_{5/2}^*$ multiplets corresponds to $\Delta_{6H_{5/2}}^{\text{CF}} = 20$ and 22 meV, respectively.

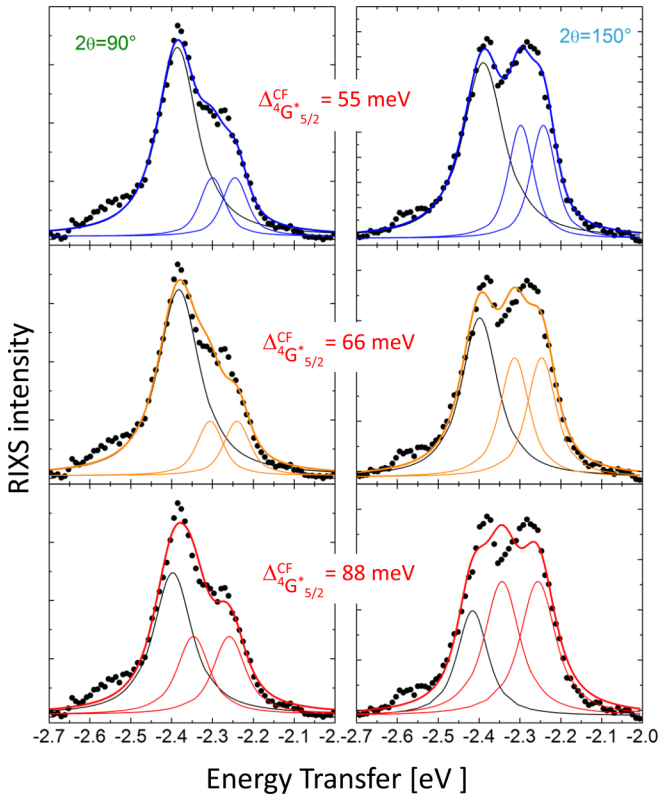


FIG. 6. Simulations with three Voigt profiles of the ${}^4F_{3/2}$ and crystal-field split ${}^4G_{5/2}^*$ multiplets measured with $2\theta = 90^\circ$ and 150° . The simulations assume different crystal-field splittings. The respective splittings are given in the panels for ${}^4G_{5/2}^*$. The splitting of the ground-state multiplet ${}^6H_{5/2}$ is 2.2 times smaller.

best fits yield $\Delta_{G_{5/2}^*}^{\text{CF}} = 43$ and 48 meV for the $2\theta = 90^\circ$ and 150° scattering configurations, respectively, corresponding to a splitting of 20 and 22 meV of the ground-state multiplet ${}^6H_{5/2}$. Other trials with larger crystal-field splittings no longer reproduce the data (see Fig. 6 in the Appendix). We learn from this exercise that $\Delta_{G_{5/2}^*}^{\text{CF}}$ ($\Delta_{H_{5/2}}^{\text{CF}}$) should be < 66 meV (< 30 meV). Summarizing, we thus find $\Delta_{H_{5/2}}^{\text{CF}} = 20 \pm 10$ meV.

V. DISCUSSION

The present RIXS result agrees surprisingly well with the CF splitting that is expected from the extrapolation within the RB_6 series [50]. The result also explains the line shape of the lowest f state signal as measured in photoemission [11]; we can now propose to describe it in terms of two Lorentzian lines, one twice as strong as the other according to a Γ_8 quartet ground state and a Γ_7 excited doublet, that are about 20 meV apart. Furthermore, the present data confirm the nonresonant inelastic x-ray scattering result of SmB_6 that also finds a quartet ground state [41,42].

The finding that the CF splitting is $10 \text{ meV} < \Delta_{H_{5/2}}^{\text{CF}} < 30 \text{ meV}$ in combination with the NIXS result that the ground state is not a highly mixed Γ_8 and Γ_7 state [41] indicates that the $4f$ bandwidth is small and less than about 20 meV, otherwise no CF splitting would have been observed. Considering the fact that the bandwidth from band-structure calculations is

several hundred meV, we infer that the mass renormalization is extremely large. This also gives credit to the idea that coefficients of fractional parentage should be considered for removing or adding an electron from/to the lowest Sm f^6 or f^5 multiplet states [71]: a reduction factor of 0.033 can be found for the f - f hopping. A Gutzwiller study uses a somewhat less strong reduction factor [22], while a DMFT calculation [43] found, indeed, the extremely narrow bands. It should be noted, however, that the sign of the CF splitting and thus also its magnitude used or found in these many-body calculations [22,43] is different from the experiment. It would be highly desirable if these calculations could be tuned in a way that they reproduce the experimental values.

It is important to recall that for the system to be an insulator, the indirect gap can be formed only if the $4f$ states have a (positive) energy dispersion [20–24]. Our finding for the upper limit for the $4f$ bandwidth is therefore consistent with the smallness of the indirect gap of SmB_6 . Moreover, renormalized band calculations showed that the topological surface states reside in this gap for an appreciable part of the surface Brillouin zone [16,21–23]. Therefore, the experimental search for the presence of topological surface states should not focus on surface states that have strong dispersions while crossing the Fermi level because these states have a very different origin.

VI. SUMMARY

The CF splitting of the ${}^6H_{5/2}$ Hund's rule ground state of Sm^{3+} in SmB_6 has been investigated with RIXS at the Sm M_5 edge. By analyzing the splitting of a multiplet at 2 eV, we find that the Γ_8 quartet forms the ground state of the ${}^6H_{5/2}$ multiplet and that the excited Γ_7 must be 20 ± 10 meV higher in energy. The impact of this finding on the energy scale of the topological surface states has been discussed.

ACKNOWLEDGMENT

A.A. and A.S. gratefully acknowledge the financial support of the Deutsche Forschungsgemeinschaft under project SE 1441-4-1.

APPENDIX

Figure 6 shows empirical descriptions of the ${}^4F_{3/2}$ and ${}^4G_{5/2}^*$ multiplets with three Voigt profiles, one for the ${}^4F_{3/2}$ and two for the crystal-field split ${}^4G_{5/2}^*$ multiplet. The Gaussian contribution was kept fixed to the instrumental resolution of 45 meV, while the Lorentzian linewidths were varied. Here the constraint was imposed that the two crystal-field excitations have the same linewidth and also the same intensity. The position of the three lines was varied with the limitation that the separation of the crystal-field excitations was set to specific values (see panels of Fig. 6). For $\Delta_{G_{5/2}^*}^{\text{CF}} = 55$ meV ($\Delta_{H_{5/2}}^{\text{CF}} = 25$ meV) both configurations are still well described with the three Voigt profiles; for $\Delta_{G_{5/2}^*}^{\text{CF}} \geq 66$ meV ($\Delta_{H_{5/2}}^{\text{CF}} \geq 30$ meV) it is no longer possible to describe the data with the scattering angle of $2\theta = 150^\circ$. This shows that the crystal-field splitting of the ground state must be smaller than 30 meV.

- [1] A. Menth, E. Buehler, and T. H. Geballe, Magnetic and Semiconducting Properties of SmB_6 , *Phys. Rev. Lett.* **22**, 295 (1969).
- [2] R. L. Cohen, M. Eibschütz, and K. W. West, Electronic and Magnetic Structure of SmB_6 , *Phys. Rev. Lett.* **24**, 383 (1970).
- [3] J. W. Allen, B. Batlogg, and P. Wachter, Large low-temperature Hall effect and resistivity in mixed-valent SmB_6 , *Phys. Rev. B* **20**, 4807 (1979).
- [4] B. Gorshunov, N. Sluchanko, A. Volkov, M. Dressel, G. Knebel, A. Loidl, and S. Kunii, Low-energy electrodynamics of SmB_6 , *Phys. Rev. B* **59**, 1808 (1999).
- [5] P. S. Riseborough, Heavy fermion semiconductors, *Adv. Phys.* **49**, 257 (2000).
- [6] N. Xu, X. Shi, P. K. Biswas, C. E. Matt, R. S. Dhaka, Y. Huang, N. C. Plumb, M. Radović, J. H. Dil, E. Pomjakushina, K. Conder, A. Amato, Z. Salman, D. McK. Paul, J. Mesot, H. Ding, and M. Shi, Surface and bulk electronic structure of the strongly correlated system SmB_6 and implications for a topological Kondo insulator, *Phys. Rev. B* **88**, 121102(R) (2013).
- [7] Z.-H. Zhu, A. Nicolaou, G. Levy, N. P. Butch, P. Syers, X. F. Wang, J. Paglione, G. A. Sawatzky, I. S. Elfimov, and A. Damascelli, Polarity-Driven Surface Metallicity in SmB_6 , *Phys. Rev. Lett.* **111**, 216402 (2013).
- [8] M. Neupane, N. Alidoust, S.-Y. Xu, T. Kondo, Y. Ishida, D. J. Kim, Chang Liu, I. Belopolski, Y. J. Jo, T.-R. Chang, H.-T. Jeng, T. Durakiewicz, L. Balicas, H. Lin, A. Bansil, S. Shin, Z. Fisk, and M. Hasan, Surface electronic structure of the topological Kondo-insulator candidate correlated electron system SmB_6 , *Nat. Commun.* **4**, 2991 (2013).
- [9] J. Jiang, S. Li, T. Zhang, Z. Sun, F. Chen, Z. R. Ye, M. Xu, Q. Q. Ge, S. Y. Tan, X. H. Niu, M. Xia, B. P. Xie, Y. F. Li, X. H. Chen, H. H. Wen, and D. L. Feng, Observation of possible topological in-gap surface states in the Kondo insulator SmB_6 by photoemission, *Nat. Commun.* **4**, 3010 (2013).
- [10] J. D. Denlinger, J. W. Allen, J.-S. Kang, K. Sun, J.-W. Kim, J. H. Shim, B. I. Min, D.-J. Kim, and Z. Fisk, Temperature dependence of linked gap and surface state evolution in the mixed valent topological insulator SmB_6 , [arXiv:1312.6637](https://arxiv.org/abs/1312.6637) (2013).
- [11] J. D. Denlinger, J. W. Allen, J.-S. Kang, K. Sun, B.-II Min, D.-J. Kim, and Z. Fisk, SmB_6 Photoemission: Past and present, *J. Phys. Jpn. Conf. Proc.* **3**, 017038 (2014).
- [12] M. C. Hatnean, M. R. Lees, D. M. K. Paul, and G. Balakrishnan, Large, high quality single-crystals of the new topological Kondo insulator, SmB_6 , *Sci. Rep.* **3**, 3071 (2013).
- [13] X. Zhang, N. P. Butch, P. Syers, S. Ziemak, R. L. Greene, and J. Paglione, Hybridization, Inter-Ion Correlation, and Surface States in the Kondo Insulator SmB_6 , *Phys. Rev. X* **3**, 011011 (2013).
- [14] D. J. Kim, S. Thomas, T. Grant, J. Botimer, Z. Fisk, and J. Xia, Surface Hall effect and nonlocal transport in SmB_6 : Evidence for surface conduction, *Sci. Rep.* **3**, 3150 (2013).
- [15] S. Wolgast, C. Kurdak, K. Sun, J. W. Allen, D. J. Kim, and Z. Fisk, Low-temperature surface conduction in the Kondo insulator SmB_6 , *Phys. Rev. B* **88**, 180405(R) (2013).
- [16] D. J. Kim, J. Xia, and Z. Fisk, Topological surface state in the Kondo insulator samarium hexaboride, *Nat. Mater.* **13**, 466 (2014).
- [17] S. Wolgast, Y. S. Eo, T. Öztürk, G. Li, Z. Xiang, C. Tinsman, T. Asaba, B. Lawson, F. Yu, J. W. Allen, K. Sun, L. Li, C. Kurdak, D.-J. Kim, and Z. Fisk, Magnetotransport measurements of the surface states of samarium hexaboride using corbino structures, *Phys. Rev. B* **92**, 115110 (2015).
- [18] S. Thomas, D. J. Kim, S. B. Chung, T. Grant, Z. Fisk, and Jing Xia, Weak antilocalization and linear magnetoresistance in the surface state of SmB_6 , *Phys. Rev. B* **94**, 205114 (2016).
- [19] Y. Nakajima, P. Syers, X. Wang, R. Wang, and J. Paglione, One-dimensional edge state transport in a topological Kondo insulator, *Nat. Phys.* **12**, 213 (2016).
- [20] M. Dzero, K. Sun, V. Galitski, and P. Coleman, Topological Kondo Insulators, *Phys. Rev. Lett.* **104**, 106408 (2010).
- [21] T. Takimoto, SmB_6 : A promising candidate for a topological insulator, *J. Phys. Soc. Jpn.* **80**, 123710 (2011).
- [22] F. Lu, J. Z. Zhao, H. Weng, Z. Fang, and X. Dai, Correlated Topological Insulators with Mixed Valence, *Phys. Rev. Lett.* **110**, 096401 (2013).
- [23] V. Alexandrov, M. Dzero, and P. Coleman, Cubic Topological Kondo Insulators, *Phys. Rev. Lett.* **111**, 226403 (2013).
- [24] M. Dzero and V. Galitski, A new exotic state in an old material: A tale of SmB_6 , *J. Exp. Theor. Phys.* **117**, 499 (2013).
- [25] E. Frantzeskakis, N. de Jong, B. Zwartsenberg, Y. K. Huang, Y. Pan, X. Zhang, J. X. Zhang, F. X. Zhang, L. H. Bao, O. Tegus, A. Varykhalov, A. de Visser, and M. S. Golden, Kondo Hybridization and the Origin of Metallic States at the (001) Surface of SmB_6 , *Phys. Rev. X* **3**, 041024 (2013).
- [26] N. Xu, C. E. Matt, E. Pomjakushina, X. Shi, R. S. Dhaka, N. C. Plumb, M. Radović, P. K. Biswas, D. Evtushinsky, V. Zabolotnyy, J. H. Dil, K. Conder, J. Mesot, H. Ding, and M. Shi, Exotic Kondo crossover in a wide temperature region in the topological Kondo insulator SmB_6 revealed by high-resolution ARPES, *Phys. Rev. B* **90**, 085148 (2014).
- [27] N. Xu, P. K. Biswas, J. H. Dil, R. S. Dhaka, G. Landolt, S. Muff, C. E. Matt, X. Shi, N. C. Plumb, M. Radovic, E. Pomjakushina, K. Conder, A. Amato, S. V. Borisenko, R. Yu, H.-M. Weng, Z. Fang, X. Dai, J. Mesot, H. Ding, and M. Shi, Direct observation of the spin texture in SmB_6 as evidence of the topological Kondo insulator, *Nat. Commun.* **5**, 4566 (2014).
- [28] P. Hlawenka, K. Siemensmeyer, E. Weschke, A. Varykhalov, J. Sánchez-Barriga, N. Y. Shitsevalova, A. V. Dukhnenko, V. B. Filipov, S. Gabáni, S. Flachbart, O. Rader, and E. D. L. Rienks, Samarium hexaboride: A trivial surface conductor, *Nat. Commun.* **9**, 517 (2018).
- [29] Y. Ohtsubo, Y. Yamashita, K. Hagiwara, S. Ideta, K. Tanaka, R. Yukawa, K. Horiba, H. Kumigashira, K. Miyamoto, T. Okuda, W. Hirano, F. Iga, and S. Kimura, Non-trivial surface states of samarium hexaboride at the (111) surface, *Nat. Commun.* **10**, 2298 (2019).
- [30] W. Ruan, C. Ye, M. Guo, F. Chen, X. Chen, G.-M. Zhang, and Y. Wang, Emergence of a Coherent In-Gap State in the SmB_6 Kondo Insulator Revealed by Scanning Tunneling Spectroscopy, *Phys. Rev. Lett.* **112**, 136401 (2014).
- [31] S. Rössler, T. H. Jang, D. J. Kim, Tjeng. L. H., Z. Fisk, S. Steglich, and F. Wirth, Hybridization gap and Fano resonance in SmB_6 , *Proc. Natl. Acad. Sci. USA* **111**, 4798 (2014).
- [32] S. Rössler, Lin Jiao, D. J. Kim, S. Seiro, K. Rasim, F. Steglich, L. H. Tjeng, Z. Fisk, and S. Wirth, Surface and electronic structure of SmB_6 through scanning tunneling microscopy, *Philos. Mag.* **96**, 3262 (2016).

- [33] L. Jiao, S. Rössler, D. J. Kim, L. H. Tjeng, Z. Fisk, F. Steglich, and S. Wirth, Hybridization gap and Fano resonance in SmB_6 , *Nat. Commun.* **7**, 13762 (2016).
- [34] Z. Li, J. Li, P. Blaha, and N. Kioussis, Predicted topological phase transition in the SmS Kondo insulator under pressure, *Phys. Rev. B* **89**, 121117(R) (2014).
- [35] B. S. Tan, Y.-T. Hsu, B. Zeng, M. Ciomaga Hatnean, N. Harrison, Z. Zhu, M. Hartstein, M. Kiourlappou, A. Srivastava, M. D. Johannes, T. P. Murphy, J.-H. Park, L. Balicas, G. G. Lonzarich, G. Balakrishnan, and Suchitra E. Sebastian, Unconventional Fermi surface in an insulating state, *Science* **349**, 287 (2015).
- [36] S. M. Thomas, Xiabin Ding, F. Ronning, V. Zapf, J. D. Thompson, Z. Fisk, and P. F. S. Rosa, Quantum Oscillations in Flux-Grown SmB_6 with Embedded Aluminum, *Phys. Rev. Lett.* **122**, 166401 (2019).
- [37] A. Yanase and H. Harima, Band calculations on YbB_{12} , SmB_6 and CeNiSn , *Prog. Theor. Phys. Suppl.* **108**, 19 (1992).
- [38] V. N. Antonov, B. N. Harmon, and A. N. Yaresko, Electronic structure of mixed-valence semiconductors in the LSDA+ U approximation. II. SmB_6 and YbB_{12} , *Phys. Rev. B* **66**, 165209 (2002).
- [39] C. J. Kang, J. Kim, K. Kim, J. Kang, J. D. Denlinger, and B. I. Min, Band symmetries of mixed-valence topological insulator: SmB_6 , *J. Phys. Soc. Jpn.* **84**, 024722 (2015).
- [40] C. N. Singh and W. C. Lee, Importance of orbital fluctuations for the magnetic dynamics in the heavy-fermion compound SmB_6 , *Phys. Rev. B* **97**, 241107(R) (2018).
- [41] M. Sundermann, H. Yavas, K. Chen, D. J. Kim, Z. Fisk, D. Kasinathan, M. W. Haverkort, P. Thalmeier, A. Severing, and L. H. Tjeng, $4f$ Crystal Field Ground State of the Strongly Correlated Topological Insulator SmB_6 , *Phys. Rev. Lett.* **120**, 016402 (2018).
- [42] Nonresonant inelastic x-ray scattering (NIXS) specifically targets the CF ground state symmetry, not the CF splitting.
- [43] J. Kim, K. Kim, C.-J. Kang, S. Kim, H. C. Choi, J.-S. Kang, J. D. Denlinger, and B. I. Min, Termination-dependent surface in-gap states in a potential mixed-valent topological insulator: SmB_6 , *Phys. Rev. B* **90**, 075131 (2014).
- [44] J. W. Allen, L. I. Johansson, I. Lindau, and S. B. Hagstrom, Surface mixed valence in Sm and SmB_6 , *Phys. Rev. B* **21**, 1335 (1980).
- [45] J. M. Tarascon, Y. Ishikawa, B. Chevalier, J. Etourneau, P. Hagenmuller, and M. Kasaya, Temperature dependence of the samarium oxidation state in SmB_6 and $\text{Sm}_{1-x}\text{La}_x\text{B}_6$, *J. Phys.* **41**, 1141 (1980).
- [46] M. Mizumaki, S. Tsutsui, and F. Iga, Temperature dependence of Sm valence in SmB_6 studied by x-ray absorption spectroscopy, *J. Phys.: Conf. Ser.* **176**, 012034 (2009).
- [47] N. P. Butch, J. Paglione, P. Chow, Y. Xiao, C. A. Marianetti, C. H. Booth, and J. R. Jeffries, Pressure-Resistant Intermediate Valence in the Kondo Insulator SmB_6 , *Phys. Rev. Lett.* **116**, 156401 (2016).
- [48] Y. Utsumi, D. Kasinathan, K.-T. Ko, S. Agrestini, M. W. Haverkort, S. Wirth, Y.-H. Wu, K.-D. Tsuei, D.-J. Kim, Z. Fisk, A. Tanaka, P. Thalmeier, and L. H. Tjeng, Bulk and surface electronic properties of SmB_6 : A hard x-ray photoelectron spectroscopy study, *Phys. Rev. B* **96**, 155130 (2017).
- [49] K. R. Lea, M. J. M. Leask, and W. P. Wolf, The raising of angular momentum degeneracy of f -electron terms by cubic crystal fields, *J. Phys. Chem. Solids* **23**, 1381 (1962).
- [50] M. Loewenhaupt and M. Prager, Crystal fields in PrB_6 and NdB_6 , *Z. Phys. B: Condens. Matter* **62**, 195 (1986).
- [51] B. Frick and M. Loewenhaupt, Crystal field spectroscopy by inelastic neutron scattering, *Z. Phys. B: Condens. Matter* **63**, 213 (1986).
- [52] E. Pellegrin, N. Nücker, J. Fink, S. L. Molodtsov, A. Gutiérrez, E. Navas, O. Strebel, Z. Hu, M. Domke, G. Kaindl, S. Uchida, Y. Nakamura, J. Markl, M. Klauda, G. Saemann-Ischenko, A. Krol, J. L. Peng, Z. Y. Li, and R. L. Greene, Orbital character of states at the Fermi level in $\text{La}_{2-x}\text{Sr}_x\text{CuO}_4$ and $\text{R}_{2-x}\text{Ce}_x\text{CuO}_4$ ($R = \text{Nd, Sm}$), *Phys. Rev. B* **47**, 3354 (1993).
- [53] P. A. Alekseev, V. N. Lazukov, R. Osborn, B. D. Rainford, I. P. Sadikov, E. S. Konovalova, and Yu. B. Paderno, Neutron scattering study of the intermediate-valent ground state in SmB_6 , *Eur. Phys. Lett.* **23**, 347 (1993).
- [54] P. A. Alekseev, J. M. Mignot, J. Rossat-Mignod, V. N. Lazukov, I. P. Sadikov, E. S. Konovalova, and Yu. B. Paderno, Magnetic excitation spectrum of mixed-valence SmB_6 studied by neutron scattering on a single crystal, *J. Phys.: Condens. Matter* **7**, 289 (1995).
- [55] W. T. Fuhrman, J. Leiner, P. Nikolić, G. E. Granroth, M. B. Stone, M. D. Lumsden, L. DeBeer-Schmitt, P. A. Alekseev, J.-M. Mignot, S. M. Koohpayeh, P. Cottingham, W. A. Phelan, L. Schoop, T. M. McQueen, and C. Broholm, Interaction Driven Subgap Spin Exciton in the Kondo Insulator SmB_6 , *Phys. Rev. Lett.* **114**, 036401 (2015).
- [56] P. A. Alekseev, J. M. Mignot, P. S. Savchenkov, and V. N. Lazukov, First evidence for a Sm^{3+} -type contribution to the magnetic form factor in the quasielastic spectral response of intermediate valence SmB_6 , *JETP Lett.* **103**, 636 (2016).
- [57] W. T. Fuhrman, J. R. Chamorro, P. A. Alekseev, J.-M. Mignot, T. Keller, J. A. Rodriguez-Rivera, Y. Qiu, P. Nikolić, T. M. McQueen, and C. L. Broholm, Screened moments and extrinsic in-gap states in samarium hexaboride, *Nat. Commun.* **9**, 1539 (2018).
- [58] A. Amorese, N. Caroca-Canales, S. Seiro, C. Krellner, G. Ghiringhelli, N. B. Brookes, D. V. Vyalikh, C. Geibel, and K. Kummer, Crystal electric field in CeRh_2Si_2 studied with high-resolution resonant inelastic soft x-ray scattering, *Phys. Rev. B* **97**, 245130 (2018).
- [59] A. Amorese, K. Kummer, N. B. Brookes, O. Stockert, D. T. Adroja, A. M. Strydom, A. Sidorenko, H. Winkler, D. A. Zocco, A. Prokofiev, S. Paschen, M. W. Haverkort, L. H. Tjeng, and A. Severing, Determining the local low-energy excitations in the Kondo semimetal CeRu_4Sn_6 using resonant inelastic x-ray scattering, *Phys. Rev. B* **98**, 081116(R) (2018).
- [60] A. Kotani and S. Shin, Resonant inelastic x-ray scattering spectra for electrons in solids, *Rev. Mod. Phys.* **73**, 203 (2001).
- [61] C. Dallera, M. Grioni, A. Shukla, G. Vankó, J. L. Sarrao, J. P. Rueff, and D. L. Cox, New Spectroscopy Solves an Old Puzzle: The Kondo Scale in Heavy Fermions, *Phys. Rev. Lett.* **88**, 196403 (2002).
- [62] H. W. Haak, G. A. Sawatzky, and T. D. Thomas, Auger-Photoelectron Coincidence Measurements in Copper, *Phys. Rev. Lett.* **41**, 1825 (1978).

- [63] E. Jensen, R. A. Bartynski, S. L. Hulbert, E. D. Johnson, and R. Garrett, Line Narrowing in Photoemission by Coincidence Spectroscopy, *Phys. Rev. Lett.* **62**, 71 (1989).
- [64] K. Hämäläinen, D. P. Siddons, J. B. Hastings, and L. E. Berman, Elimination of the Inner-Shell Lifetime Broadening in X-Ray-Absorption Spectroscopy, *Phys. Rev. Lett.* **67**, 2850 (1991).
- [65] P. Carra, M. Fabrizio, and B. T. Thole, High Resolution X-Ray Resonant Raman Scattering, *Phys. Rev. Lett.* **74**, 3700 (1995).
- [66] Here $\check{A}_k^m = A_k^m \langle r^k \rangle$, with $\langle r^k \rangle$ the expectation value of the radial part of the matrix element.
- [67] N. B. Brookes, F. Yakhou-Harris, K. Kummer, A. Fondacaro, J. C. Cezar, D. Betto, E. Velez-Fort, A. Amorese, G. Ghiringhelli, L. Braicovich, R. Barrett, G. Berruyer, F. Cianciosi, L. Eybert, P. Marion, P. van der Linden, and L. Zhang, The beamline ID32 at the ESRF for soft x-ray high energy resolution resonant inelastic x-ray scattering and polarization dependent x-ray absorption spectroscopy, *Nucl. Instrum. Methods Phys. Res. A* **903**, 175 (2018).
- [68] M. W. Haverkort, M. Zwierzycki, and O. K. Andersen, Multiplet ligand-field theory using Wannier orbitals, *Phys. Rev. B* **85**, 165113 (2012).
- [69] M. W. Haverkort, Quanta for core level spectroscopy—excitons, resonances and band excitations in time and frequency domain, *J. Phys.: Conf. Ser.* **712**, 012001 (2016).
- [70] R. D. Cowan, *The Theory of Atomic Structure and Spectra* (University of California, Berkeley, 1981).
- [71] G. Sawatzky and R. Green, The Explicit Role of Anion States in High-Valence Metal Oxides, in *Quantum Materials: Experiments and Theory*, edited by E. Pavarini, E. Koch, J. van den Brink, and G. Sawatzky (Forschungszentrum Jülich, Germany, 2016), p. 1.1.